



### Science Arts & Métiers (SAM)

is an open access repository that collects the work of Arts et Métiers Institute of Technology researchers and makes it freely available over the web where possible.

This is an author-deposited version published in: <https://sam.ensam.eu>  
Handle ID: <http://hdl.handle.net/10985/20023>

#### To cite this version :

Aurélien MACRON, Jennifer DORIDAM, Isabelle RIVALS, Mohammad Javad SADEGHINIA, Alexandre VERNEY, Pierre-Yves ROHAN, Helene PILLET - Is a simplified Finite Element model of the gluteus region able to capture the mechanical response of the internal soft tissues under compression? - Clinical Biomechanics - Vol. 71, p.92-100 - 2020

Any correspondence concerning this service should be sent to the repository

Administrator : [scienceouverte@ensam.eu](mailto:scienceouverte@ensam.eu)



# Is a simplified Finite Element model of the gluteus region able to capture the mechanical response of the internal soft tissues under compression?

Aurélien Macron<sup>a,c</sup>, Hélène Pillet<sup>a</sup>, Jennifer Doridam<sup>a</sup>, Isabelle Rivals<sup>d,e</sup>,  
Mohammad Javad Sadeghinia<sup>a,f</sup>, Alexandre Verney<sup>b</sup>, Pierre-Yves Rohan<sup>a,\*</sup>

<sup>a</sup> Institut de Biomécanique Humaine Georges Charpak, Arts et Métiers ParisTech, 151 bd de l'Hôpital, 75013 Paris, France

<sup>b</sup> CEA, LIST, Interactive Robotics Laboratory, F-91191 Gif-sur-Yvette, France

<sup>c</sup> Univ. Grenoble Alpes, CEA, LETI, CLIMATEC, MINATEC Campus, 38000 Grenoble, France

<sup>d</sup> Sorbonne Université, INSERM, UMRS1158 Neurophysiologie Respiratoire Expérimentale et Clinique, Paris, France

<sup>e</sup> Equipe de Statistique Appliquée, ESPCI Paris, PSL Research University, Paris, France

<sup>f</sup> School of Mechanical Engineering, College of Engineering, University of Tehran, Tehran, Iran

---

## A B S T R A C T

### Keywords:

Deep Tissue Injury  
Pressure Ulcer  
Subject specific  
Buttock  
Sitting  
Finite Element analysis

**Background:** Internal soft tissue strains have been shown to be one of the main factors responsible for the onset of Pressure Ulcers and to be representative of its risk of development. However, the estimation of this parameter using Finite Element (FE) analysis in clinical setups is currently hindered by costly acquisition, reconstruction and computation times. Ultrasound (US) imaging is a promising candidate for the clinical assessment of both morphological and material parameters.

**Method:** The aim of this study was to investigate the ability of a local FE model of the region beneath the ischium with a limited number of parameters to capture the internal response of the gluteus region predicted by a complete 3D FE model. 26 local FE models were developed, and their predictions were compared to those of the patient-specific reference FE models in sitting position.

**Findings:** A high correlation was observed ( $R = 0.90$ ,  $p\text{-value} < 0.01$ ). A sensitivity analysis showed that the most influent parameters were the mechanical behaviour of the muscle tissues, the ischium morphology and the external mechanical loading.

**Interpretation:** Given the progress of US for capturing both morphological and material parameters, these results are promising because they open up the possibility to use personalised simplified FE models for risk estimation in daily clinical routine.

---

## 1. Introduction

Pressure Ulcers (PU) are painful, slow-healing wounds that develop during periods of prolonged immobility, and that are likely to deteriorate the quality of life of people with poor mobility and sensitivity. They can develop either superficially and progress inward or initiate at the deep tissues and progress outward (called Deep Tissue Injury) depending on the nature of the surface loading (Bouten et al., 2003). The first type is predominantly caused by shear stresses and is fairly easily detected and treated before it becomes dangerous. The latter type, caused by sustained compression of the tissue, originates subcutaneously, generally close to bony prominences (NPUAP/EPUAP, 2009). Although DTI represents a small proportion of PUs ( $< 10\%$ ) this latter type is considered especially harmful because layers of muscle,

fascia, and subcutaneous tissue may suffer substantial necrosis equivalent to a category III or IV PU with variable prognosis.

Since the pioneer work of Daniel et al. (1981), Kosiak (1961), and Reswick and Rogers (1976) establishing the dependence of PU development on both external pressure and time, interface pressure mapping has been widely used in PU prevention. Although clinically useful, interface pressure monitoring is not predictive enough of the risk of PU development. Indeed, it is now indisputable that there are at least two damage mechanisms, which play an important role in PU development (Oomens et al., 2015): (i) mechanically induced capillary occlusions that lead to low oxygen concentration in the tissue triggering a cascade of inflammatory signals that culminate in ulceration (Gawlitta et al., 2007; Kosiak, 1959; Loerakker et al., 2011; Sree et al., 2019a). This process can occur even for very small values of soft tissue strain and

---

\* Corresponding author.

E-mail address: pierre-yves.rohan@ensam.eu (P.-Y. Rohan).

takes several hours before the first signs of cell damage can be detected (Breuls et al., 2003; Loerakker et al., 2010; Stekelenburg et al., 2007, 2006). (ii) “direct deformation damage” involving cells damage by direct (shear) deformation (Breuls et al., 2003; Ceelen et al., 2008; Stekelenburg et al., 2006). This damage can be evident when the threshold for deformation damage exceeds the normal physiological values experienced in daily life and can be detected in a period of minutes (Ceelen et al., 2008; Loerakker et al., 2010). In addition, microclimate (skin surface temperature and skin moisture) is also suspected to play a key role in PU causation (Gefen, 2011; Zeevi et al., 2017) but the extent of the contribution and its interaction with sustained tissue deformations have yet to be quantified.

Estimating the internal mechanical conditions within loaded soft tissues has the potential of improving the management and prevention of PU and several Finite Element (FE) models have been developed for > 20 years to bridge the gap between external pressures and internal strains (Al-Dirini et al., 2016; Linder-Ganz et al., 2009; Luboz et al., 2017; Moerman et al., 2017). Along these lines, we recently proposed a new methodology to build a 3D patient-specific FE model based on the combination of ultrasound (US), bi-planar x-ray radiographies and optical scanner (Macron et al., 2018) to estimate internal strains in sitting position. However, the clinical use of such models is currently hindered by costly acquisition, reconstruction and computation times. In contrast, there is a consensus in the results reported in the literature that the clinically relevant mechanical response is localised under the ischium. This strongly suggests that a local model of the soft tissue under the ischium could account for the major part of the mechanisms. Recent evidence also suggest that response to damage, as observed by MRI, starts at some distance from the deformation (Nelissen et al., 2018), highlighting the importance of evaluating the mechanical response in 3 dimensions.

Only a few contributions have tried to explore this avenue in the literature. In 2011, Portnoy et al. developed a simple 2D analytical model (Portnoy et al., 2011) based on the Hertz contact model. Promising results have been reported regarding the comparison between the maximal Von Mises stress estimated by their local model and that predicted by a full 3D FE model developed by Linder-Ganz et al. (2008). In a sample of 11 healthy subjects, a Pearson correlation of 0.4 was obtained. However, the consistency of the results can be expected to be improved by adding complementary parameters that have been identified as predominant in the internal mechanical response of the ischial region, such as the radius of the ischium (Agam and Gefen, 2007) and the mechanical behaviour of the soft tissue (Luboz et al., 2014). Moreover, shear strains estimations also seem essential and were not reported in their work. Thus, there is a need to extend this analytical approach to a more comprehensive model of the behaviour of the soft tissue in the ischial region with the additional constraint that it should be based on parameters that can be routinely obtained in a clinical environment.

At the same time, recent studies showed the potential of US imaging for the characterization of morphological parameters. In a recent paper, Akins et al. reported that the measurement of the adipose and muscle tissue thicknesses in the vicinity of the ischium using US was both reliable (ICC = 0.948) and highly correlated with MRI assessment ( $r = 0.988$  and  $0.894$  for the muscle and the adipose tissues respectively) (Akins et al., 2016). On the contrary, the measurement of the radius of curvature of the ischium was reported to have a poor inter operator reliability be it using US (ICC =  $-0.028$ ) (Akins et al., 2016) or MRI (ICC = 0.214) (Swaine et al., 2017). However, there is a high interest in the community for developing both the US system (Bercoff et al., 2004; Gennisson et al., 2013, 2010) and clinical protocols that are suited to reliable parameter assessment (Swaine et al., 2017). Similar efforts are being made to characterize material parameters (Makhsous et al., 2008). This makes US a promising candidate to substitute MR imaging for clinically feasible assessment of both morphological and material parameters needed for the prevention of PU.

In this perspective, we propose here to evaluate the ability of a local model of the region beneath the ischium to capture the maximum shear strain inside the muscle tissue. This evaluation will be made by comparing the response provided by this model to the one predicted by a previously developed complete 3D FE model of the buttock (Macron et al., 2018). In addition, the relative impact of the different parameters on the local model response will be analysed.

## 2. Methods

For the sake of clarity, the experimental material and the construction of the reference FE model (Macron et al., 2018) are briefly recalled hereunder in Section 2.1.

### 2.1. Reference FE model

13 subject-specific FE models (8 men and 5 women; age:  $26 \pm 5$  years, weight:  $70 \pm 9$  kg, BMI:  $22.6 \pm 3.4$  kg/m<sup>2</sup>) models (reference) were generated from previous experiments detailed in Macron et al. (2018).

3D reconstruction of the pelvis was performed from biplanar X-rays in an unloaded sitting position. The external envelope was reconstructed from the optical scan acquisition, and the adipose tissue thickness was directly measured on the US image in the unloaded configuration.

The skin, fat and muscle tissues were each modelled with a first order Ogden hyperelastic material model (Simo and Taylor, 1991). Material parameters for the skin were based on values reported in the literature (Luboz et al., 2014). For the fat and the muscle,  $\alpha$  was arbitrarily fixed to 5 (Oomens et al., 2016) and the shear modulus  $\mu$  was calibrated using Finite Element Updating to fit the experimental ischial tuberosity sagging (Macron et al., 2018). The shear moduli of the adipose and muscle tissue will subsequently be referred to as  $\mu_F$  and  $\mu_M$ .

For the boundary conditions, all the degrees of freedom (DOF) of the pelvis were fixed except the vertical displacement. The experimental vertical force measured in the loaded sitting position was applied at the centre of mass of the pelvis.

The nodes at the different interfaces (bone/muscle, muscle/fat, and fat/skin) of the model were tied. A friction contact between the rigid plane and the skin surface was defined using a penalty algorithm. The friction coefficient was set to 0.4 (Al-Dirini et al., 2016).

### 2.2. Local FE model

#### 2.2.1. Extraction of model parameters

The parameters necessary for the construction of the local FE model were quantified for the 13 subjects.

Two radii of curvature were calculated from the 3D pelvis reconstruction. For each side of the pelvis, the extreme node of the surface mesh with the lowest vertical coordinate was identified. A region of interest containing all the nodes at < 8 mm of the extreme node was then defined. Several planes containing the vertical direction were generated. The orientation of their normal vectors was distributed between 0 and 170 degrees by 10 degree increments. Each plane intersected the region of interest and allowed to define a set of nodes which were used to extract a radius from a circular regression. The minimal radius obtained across the planes is called  $R1$ . The radius of curvature  $R2$  in the orthogonal plane was then extracted.

The fat thickness  $eF$  was extracted from the US image in the unloaded sitting position. The total subdermal soft tissue thickness under the ischium was extracted from the sagittal x-ray image in the unloaded sitting position, and the muscle thickness  $eM$  was calculated as the difference between the total thickness and the fat thickness.

The static contact pressure distribution at the skin/seat interface computed by the reference FE model in the loaded sitting position was used to extract the net reaction force. The pressure distribution was first

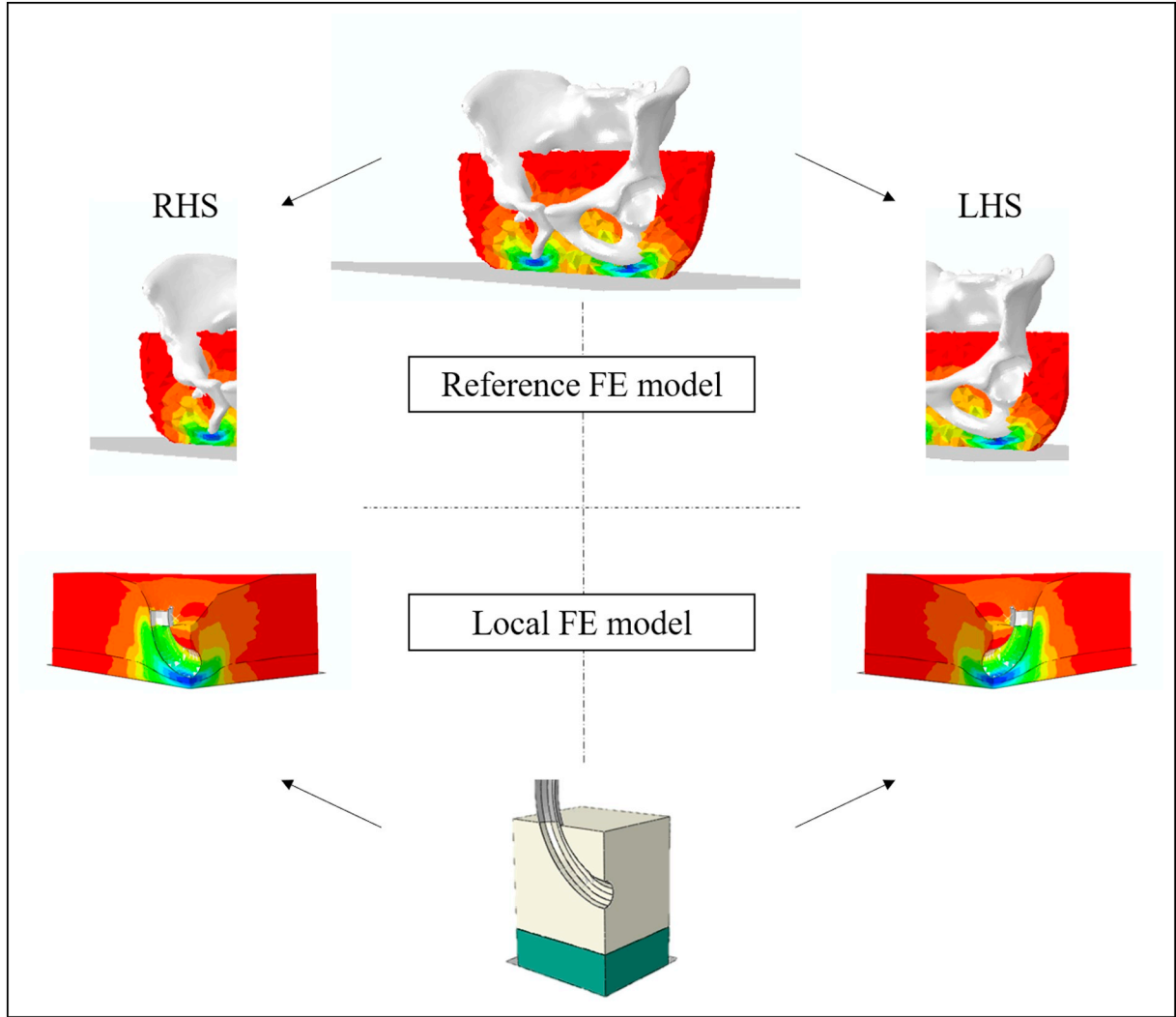


Fig. 1. Reference FE model (top) and associated LHS and RHS local FE models (bottom) for one subject.

interpolated over a regular grid with 1 mm spatial resolution. The contact pressure of the nearest FE surface node of the reference model was assigned to each point of the grid. The nodal vector force associated to each grid node was then computed by multiplying the nodal pressure with the surface area ( $1 \text{ mm}^2$ ). A net reaction force  $\mathbf{F}$  was calculated as the vector sum of the nodal forces on the left-hand side (LHS) and right-hand side (RHS).

To summarize, seven parameters were considered:  $\mu F$ ,  $\mu M$ ,  $R1$ ,  $R2$ ,  $eF$ ,  $eM$ ,  $F$ .

### 2.2.2. Finite Element modelling

26 local FE models were developed to represent the mechanical response of the LHS and RHS of the 13 patient-specific reference FE models (Fig. 1).

The local FE model geometry is presented in Fig. 2. The ischial tuberosity is represented by a torus generated by the revolution of a parametric curve  $C$  containing a portion of a circle of radius  $R2$  swept by a semi-disc of radius  $R1$ . A box of height  $h$ , length  $L$  and width  $L$  was defined to represent the whole subdermal soft tissue (fat + muscle). A convergence study showed that, above an  $L/h$  ratio of 2, the solution was not affected. A boolean operation was performed to subtract the ischium from the soft tissue volume. A skin layer of 1 mm thickness was defined. A rigid horizontal plane was created to model the seat support.

The soft tissues were meshed using linear tetrahedral elements with hybrid formulation (C3D4H) in ABAQUS Finite Element Analysis

software (ABAQUS Inc., Providence, RI, USA). The pelvis was assumed to be rigid and meshed with triangular shell elements. The same constitutive laws and material parameters as those defined in Section 2.1 for the reference FE model were used for each subject. Likewise, for the boundary conditions, all the DOF of the ischium were fixed except the vertical displacement. The force  $\mathbf{F}$  was applied to the ischium. Only a quarter of the model was considered and the remainder was completed using the symmetry constraints (Fig. 2).

### 2.2.3. Quantity of interest

The strains were post-processed from the principal stretches  $\lambda_i$  ( $i = 1, 2, 3$ ). Based on these, the principal Green-Lagrange strains were calculated as:  $E_i = \frac{(\lambda_i^2 - 1)}{2}$  and the principal shear strains were then computed as:

$$E_{shear} = \frac{1}{2} * \max(|E_1 - E_2|, |E_2 - E_3|, |E_3 - E_1|)$$

The third principal strain component  $E_3$  corresponds to the principal compressive strain. This quantity will be referred to hereafter as  $E_{comp}$ .

In line with Bucki et al. (2016) and Luboz et al. (2017), a “cluster analysis” was performed to investigate volumes of the model that are in given intervals of maximum shear strain. Clusters were defined as the union of adjacent elements verifying the following criteria: (i)  $E_{shear}$  above 75% and (ii)  $E_{comp}$  above 45%. These correspond to the damage thresholds reported by Ceelen et al. (2008) for the muscle tissue.

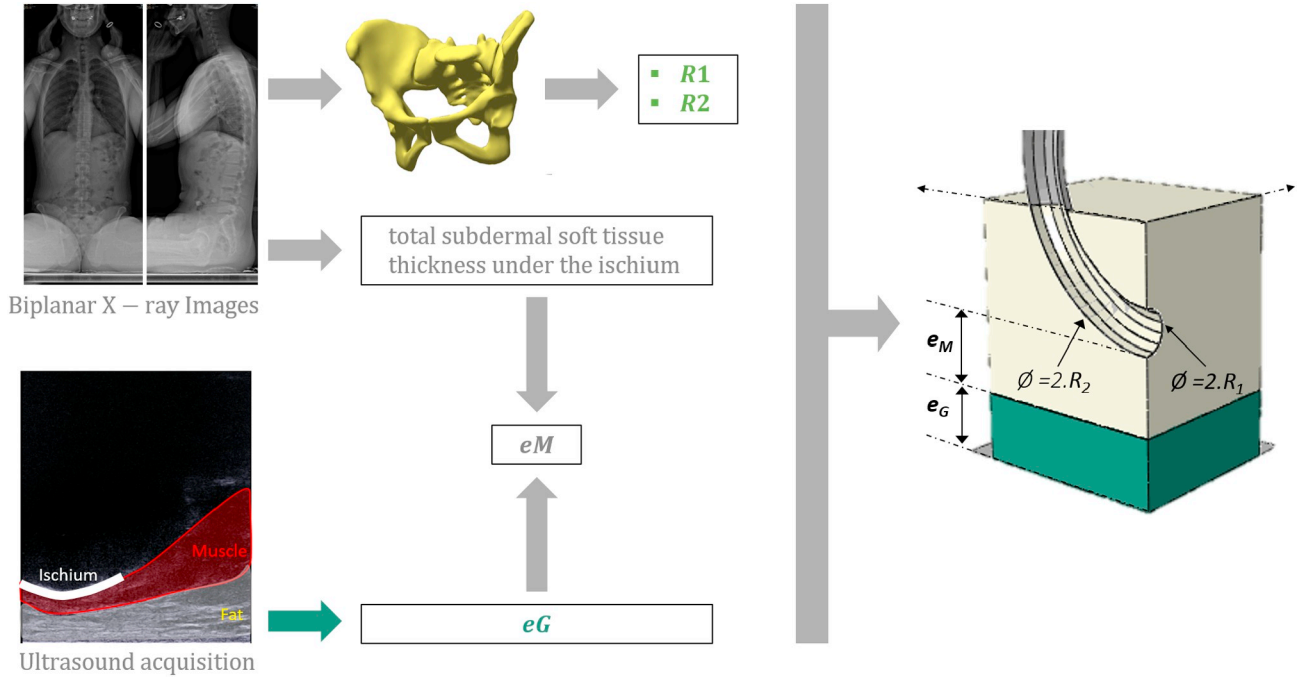


**Fig. 2.** Local FE model geometry generated from the 4 geometric parameters  $R1$ ,  $R2$ ,  $eF$ ,  $eM$  extracted from the ultrasound and bi-planar x-ray images. The ischial tuberosity is represented by a torus generated by the revolution of a circle of radius  $R1$  (minor radius of the torus) around a portion of a circle of radius  $R2$  (major radius of the torus).  $eM$  and  $eF$  are used to define the muscle and fat thicknesses respectively.

However, unlike Bucki et al. (2016) who investigated the response in both muscle and fat, only the muscle tissue was investigated here.

To be able to compare our results with those of the literature, the Engineering strain was defined as follows:  $\epsilon_i = \lambda_i - 1$ . As previously, the principal shear strains were computed from the principal Engineering strains:

$$\epsilon_{shear} = \frac{1}{2} * \max(|\epsilon_1 - \epsilon_2|, |\epsilon_2 - \epsilon_3|, |\epsilon_3 - \epsilon_1|)$$

For the reference FE model, the maximum principal shear strain  $\epsilon_{max} = \max(\epsilon_{shear})$  in the cluster with the largest volume inside the muscle tissue was extracted and analysed. For the local FE model, the maximum principal shear strain  $\epsilon_{max} = \max(\epsilon_{shear})$  was computed from the elements inside the muscle tissue and on the axis of symmetry.

### 2.3. Correlation between the reference and the local model

The correlation between the maximum principal shear strain predictions of the reference and local FE models was quantified with Pearson's correlation coefficient on the 13 patients (left and right).

### 2.4. Sensitivity analysis of the local model

In order to investigate the impact of the input parameters ( $R1$ ,  $R2$ ,

**Table 1**  
Levels of the parameters used for the sensitivity analysis.

| Parameter | Level of the parameter |           |                |
|-----------|------------------------|-----------|----------------|
|           | Min level (-1)         | Mid-level | Max level (+1) |
| $R1$      | 5 (mm)                 | 7 (mm)    | 9 (mm)         |
| $R2$      | 15 (mm)                | 39 (mm)   | 63 (mm)        |
| $eM$      | 19 (mm)                | 29 (mm)   | 39 (mm)        |
| $eG$      | 9 (mm)                 | 22 (mm)   | 35 (mm)        |
| $\mu M$   | 1.0 (kPa)              | 4.5 (kPa) | 8.0 (kPa)      |
| $\mu G$   | 2.8 (kPa)              | 5.4 (kPa) | 8.0 (kPa)      |
| $F$       | 48 (N)                 | 77.5 (N)  | 107 (N)        |

$eM$ ,  $eF$ ,  $\mu M$ ,  $\mu F$  and  $F$ ) on the maximum shear strain predicted by the local model, we chose to emulate the latter with a polynomial model using the same parameters. The ranges over which the  $m = 7$  parameters were to be varied were defined between their minimum and maximum value observed in the 13 subjects (LHS and RHS), see Table 1. After normalization in  $[-1; 1]$ , experimental points were chosen according to a three-level full factorial design resulting in  $3^7$  combinations (i.e. 2187 FE model simulations).

The output of the local FE model being noiseless, there is in principle no lower bound to the mean squared residuals of candidate models other than zero. In the following, a polynomial model of degree at most equal to two will be used:

$$y(\theta) = \theta_0 + \sum_{i=1}^m \theta_i x_i + \sum_{i=1}^m \theta_{ii} (x_i)^2 + \sum_{i=1}^m \sum_{j>i}^m \theta_{ij} x_i x_j$$

The maximum value of two for the degree will be justified in Section 2.2 of the results using the errors of the local FE model with respect to the reference FE model obtained on the 13 subjects (left and right).

The sensitivity of the model to each input (linear term, square, order-two interaction) can be simply defined as the percentage of variance due to this input. Assuming the parameters ( $R1$ ,  $R2$ ,  $eM$ ,  $eF$ ,  $\mu M$ ,  $\mu F$  and  $F$ ) independent and uniformly distributed in  $[-1, 1]$  (i.e. with second and fourth order moments of respectively  $1/3$  and  $4/45$ ), we have:

$$\left\{ \begin{array}{l} s_i = \text{var}(\theta_i x_i) = \theta_i^2 \text{var}(x_i) = \theta_i^2 \times \frac{1}{3} \\ s_i = \text{var}(\theta_{ii} x_i^2) = \theta_{ii}^2 \text{var}(x_i^2) = \theta_{ii}^2 \times \frac{4}{45} \\ s_{ij} = \text{var}(\theta_{ij} x_i x_j) = \theta_{ij}^2 \text{var}(x_i) \text{var}(x_j) = \theta_{ij}^2 \times \frac{1}{9} \\ \text{var}(y) = \sum_{i=1}^m s_i + \sum_{i=1}^m s_{ii} + \sum_{i=1}^m \sum_{j>i}^m s_{ij} \end{array} \right.$$

For the degree 1 model, the sensitivity to the  $i$ -th parameter is hence given by the following percentage:

**Table 2**

Characteristics of subjects for each side (right and left). The LHS of subject #8 is indicated in a different color because the simulation of the local FE model did not converge.

| Subject | Side | R1 (mm) | R2 (mm) | eM (mm) | eF (mm) | $\mu M$ (kPa) | $\mu F$ (kPa) | F (N) |
|---------|------|---------|---------|---------|---------|---------------|---------------|-------|
| #1      | R    | 6.9     | 19.7    | 28      | 10      | 8.00          | 5.00          | 196   |
|         | L    | 7.1     | 22.8    | 31      | 10      | 8.00          | 5.00          | 258   |
| #2      | R    | 6.9     | 20.3    | 26      | 33      | 4.80          | 3.75          | 251   |
|         | L    | 6.9     | 20.8    | 27      | 33      | 4.80          | 3.75          | 251   |
| #3      | R    | 8.5     | 18.9    | 31      | 19      | 6.25          | 3.75          | 324   |
|         | L    | 7.2     | 19.1    | 26      | 19      | 6.25          | 3.75          | 378   |
| #4      | R    | 7.0     | 24.8    | 26      | 14      | 8.00          | 6.25          | 329   |
|         | L    | 7.3     | 28.8    | 25      | 14      | 8.00          | 6.25          | 237   |
| #5      | R    | 6.7     | 20.3    | 21      | 11      | 8.00          | 2.75          | 194   |
|         | L    | 6.8     | 22.2    | 21      | 11      | 8.00          | 2.75          | 218   |
| #6      | R    | 6.9     | 22.8    | 21      | 25      | 8.00          | 8.00          | 244   |
|         | L    | 7.0     | 21.5    | 24      | 25      | 8.00          | 8.00          | 334   |
| #7      | R    | 7.0     | 29.9    | 28      | 9       | 8.00          | 2.75          | 302   |
|         | L    | 8.9     | 15.2    | 33      | 9       | 8.00          | 2.75          | 211   |
| #8      | R    | 6.7     | 18.1    | 29      | 22      | 1.00          | 4.50          | 246   |
|         | L    | 7.2     | 21.3    | 29      | 22      | 1.00          | 4.50          | 288   |
| #9      | R    | 7.3     | 30.3    | 19      | 35      | 4.50          | 2.75          | 429   |
|         | L    | 6.5     | 63.3    | 29      | 35      | 4.50          | 2.75          | 232   |
| #10     | R    | 5.5     | 52.1    | 36      | 23      | 2.75          | 4.50          | 268   |
|         | L    | 7.1     | 21.0    | 39      | 23      | 2.75          | 4.50          | 211   |
| #11     | R    | 7.0     | 24.0    | 38      | 30      | 6.25          | 6.25          | 296   |
|         | L    | 7.8     | 21.0    | 38      | 30      | 6.25          | 6.25          | 387   |
| #12     | R    | 4.8     | 30.2    | 22      | 16      | 4.50          | 2.75          | 305   |
|         | L    | 5.3     | 34.9    | 24      | 16      | 4.50          | 2.75          | 251   |
| #13     | R    | 7.3     | 27.1    | 22      | 12      | 6.25          | 4.50          | 223   |
|         | L    | 7.4     | 33.0    | 22      | 12      | 6.25          | 4.50          | 242   |

$$S_i = \frac{s_i}{\text{var}(y)} = \frac{\theta_i^2}{\sum \theta_i^2}$$

For the degree 2 model, the sensitivities to the  $i$ -th parameter and to its interaction with parameter  $j$  are given by the percentages:

$$S_i = \frac{s_i + s_{ij}}{\text{var}(y)}, S_{ij} = \frac{s_{ij}}{\text{var}(y)}$$

### 3. Results

#### 3.1. Subjects and parameters

The values of the parameters for the 13 modelled subjects are reported in Table 2 below for each side. The simulation of the local FE model corresponding to the LHS of subject #8 did not converge.

#### 3.2. Maximum shear strains and external pressures

The bar plot below (Fig. 3) summarizes the maximum principal shear strains estimated by the reference FE model and the local FE model for each subject and for each side (right and left). In addition, the external pressure is also plotted with a secondary axis.

As shown in Fig. 3, the external pressure is poorly correlated to the maximum principal shear strain estimated by the two FE models. For example, subject #10 endures a low pressure on both sides, but suffers high internal strains. On the contrary, subject #1's left side shows a high pressure associated to a small internal strain.

Pearson's correlation coefficient between  $\varepsilon_{\max}$  estimated by the reference and local FE models was 0.90 ( $p < 0.01$ ). In contrast, Pearson's correlation coefficient between  $\varepsilon_{\max}$  estimated by the reference model and the external pressure was 0.43 ( $p = 0.03$ ).

The results depicted in Fig. 4(b) show a high linear correlation

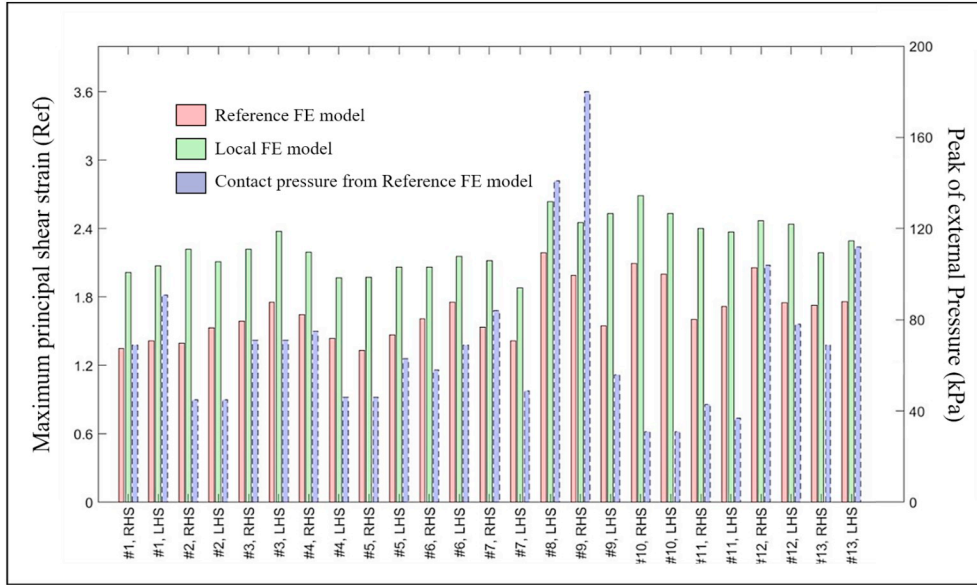


Fig. 3. Bar plots representing the maximum shear strains estimated by the local FE model (green) and the reference FE model (red), and the external pressure (blue). (For interpretation of the references to color in this figure legend, the reader is referred to the web version of this article.)

between the local FE model and the reference FE model, but a poor agreement: the mean squared error between reference and local model predictions equals 0.25. Note that for the sensitivity analysis using a polynomial model emulating the local FE models, since their outputs are noiseless, we need a lower limit for the mean square error between local model and polynomial outputs for the choice of the adequate polynomial complexity. Since even a constant model has smaller mean squared residuals (0.075) than the local FE models, their mean square error of 0.25 cannot be used to select the degree of the polynomial model emulating the local model.

However, considering the good linear correlation between the local and the reference model, we can compute the mean squared error obtained after regressing the reference model on the local one, which represents the error achieved by the local model if it were in agreement with the reference model. Thus, it provides a lower limit for the mean squared residuals of candidate polynomial models for the emulation of the local FE model. Numerically, this corrected mean squared error equals  $5.7 \cdot 10^{-3}$ .

Table 3

First order sensitivities to the 7 parameters in decreasing order of magnitude.

| Parameters | Coefficient $\theta_i$ | $Si$ (%) |
|------------|------------------------|----------|
| $\mu M$    | -0.1770                | 38       |
| $RCCI2$    | -0.1604                | 31       |
| $F$        | +0.1226                | 18       |
| $RCCI1$    | -0.1092                | 10       |
| $eM$       | +0.0213                | 0.55     |
| $eF$       | +0.0184                | 0.41     |
| $\mu G$    | -0.0178                | 0.39     |

### 3.3. Sensitivity analysis

Out of the 2187 simulations, 239 did not converge (11%). A possible reason may be the chosen values for the minimum and maximum parameter values, the minimum muscle shear modulus value in particular. Indeed, a single experimental measure was used to calibrate the

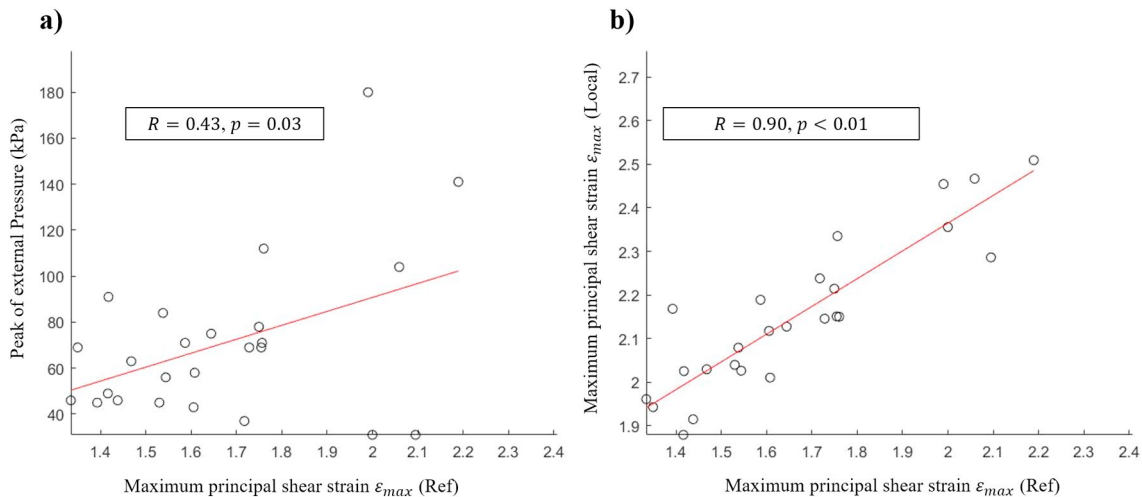


Fig. 4. (a) Maximum principal shear strains estimated by the reference FE model versus external pressure for the thirteen subjects, (b) maximum principal shear strains estimated by the reference FE model versus the predictions of the local FE model.

**Table 4**  
Second-order sensitivities (> 1%) in decreasing order of magnitude.

| Parameters   | Coefficients $\theta_i$ , $\theta_{ii}$ or $\theta_{ij}$ | $S_i$ (%) |
|--------------|--|-----------|
| $\mu M$      | -0.1662, -0.0547   | 33        |
| $RCCI2$      | -0.1632, +0.0985   | 29        |
| $F$          | +0.1068, -0.0425   | 16        |
| $RCCI1$      | -0.0817, + 0.0223  | 8.9       |
| $\mu M * eM$ | -0.1153  | 4.5       |
| $\mu M * F$  | +0.1080  | 3.7       |
| $\mu M * eF$ | -0.0607  | 1.3       |

material properties of both muscle and adipose tissues by an inverse method. Using the remaining simulations, the coefficients of the degree 1 and degree 2 models were estimated with ordinary least squares. The first order sensitivities to the 7 parameters obtained with the linear model are given in Table 3, in decreasing order of sensitivity.

The mean squared residuals of the linear model ( $2.0 * 10^{-2}$ ) largely exceeded the corrected mean squared error of  $5.7 * 10^{-3}$  obtained with the comparison to the reference model, so that first order sensitivities might not capture the complexity of the local FE model. Thus, we computed the sensitivities obtained with the second-degree model, see Table 4. Since its mean squared residuals ( $3.9 * 10^{-3}$ ) are close to the corrected mean squared error, this model is neither too simple, nor excessively complex. Note that, due to the missing data corresponding to the simulations that did not converge, the experiment matrix is not strictly orthogonal, hence the slight modification of the linear coefficients  $\theta_i$  when adding the interactions and the squared terms.

#### 4. Discussion

The aim of this study was to investigate the ability of a local model of the region beneath the ischium to capture the internal response of the buttock soft tissues predicted by a complete 3D FE model from a limited number of parameters. Our long term ambition is to take advantage of the potential of basic US for the measurement of both morphological and material parameters in daily clinical routine. To this end, we also investigated the relative impact of the main parameters reported in the literature to drive the internal response of the soft tissues.

The analysis of the results obtained in this contribution shows the biomechanical response of the internal soft tissues predicted by a local FE model in 13 subjects is similar to the one predicted by the complete and complex reference 3D FE model (Pearson coefficient of 0.90 and  $p$ -value < 0.01). Previous attempts to develop and evaluate simplified models built from a limited number of parameters have been reported in the literature (Agam and Gefen, 2007; Oomens et al., 2003; Portnoy et al., 2011). Some of these models focused on analytical solutions of the Hertz contact problem to predict both the peak interface contact pressure at the bone/muscle interface (Agam and Gefen, 2007) and the internal von Mises soft tissue stresses (Portnoy et al., 2011), and displayed a relatively good agreement with patient-specific FE von Mises stresses published by Linder-Ganz et al. on the same 11 patients ( $R = 0.4$ ) with a relatively low computation time facilitating real-time operation and portability. However, they rely on important assumptions: elasticity of the two contacting bodies, relatively small area of contact in comparison to the size of the geometry modelled. These assumptions particularly hinder models ability to estimate shear strain in the soft tissue, identified as the primary cause of soft tissue breakdown in both animal models and tissue engineered constructs at the cell level. The high correlation obtained in our contribution between the local FE model and the reference FE model for the estimation of the principal shear strain is very promising because, for the first time, it allows to consider the use of such personalised simplified models in daily clinical setup. Moreover, the results obtained in this study confirmed previous observations reported in the literature that external contact pressures are poorly correlated ( $R = 0.43$ ,  $p = 0.3$ ) to the internal local strains

endured by soft tissues (Bouten et al., 2003; Chow and Odell, 1978; Dabnichki et al., 1994; Luboz et al., 2014).

The sensitivity analysis establishes that the most influential parameter is the mechanical behaviour of the muscle soft tissue, which is in agreement with the conclusion of Luboz et al. (2014). In particular, the authors observed that a variation of Young's modulus of the muscle between 40 kPa and 160 kPa resulted in a variation of the maximum Von Mises strain of 38.5%. In our study, the shear modulus of the muscle explained 33% of the internal soft tissue response variance. We also observed that changing the mechanical properties of the underlying adipose tissue did not influence the mechanical response of the muscle tissue. This had already been reported by Oomens et al. (2003). From a clinical perspective, this result supports recent findings that SCI patients with fat infiltration, scarring or spasms puts them at a higher risk for DTI because of increased internal loads in the gluteus muscles in the vicinity of the ischial tuberosities during sitting (Sophor et al., 2011). The maximum shear strain in the muscle tissue is also very sensitive (29%) to the radius of curvature (R2) in the plane perpendicular to the shortest radius of curvature (R1) referred to as radius of curvature in the long axis by Swaine et al. (2017). This result could be expected because in indentation-like configurations, the geometry of the indenter is known to have a paramount importance. This observation could explain the increasing enthusiasm of the community for the measurement of this anatomical feature-related risk factor using medical imaging (Akins et al., 2016; Linder-Ganz et al., 2008; Swaine et al., 2017). In the literature however, only Swaine et al. (2017) represented the ischium using two radii of curvature. Our results confirm that this is essential to consider the variability along both axes in order to properly capture the mechanical response of the soft tissue. The external force explains 16% of the variability of the response. Unlike the other parameters, its measurement is relatively easy even in clinical routine. A particular attention should be paid to the extraction of the force that is transferred to the ischium from the global measurement base on pressure mattresses. Adding the smallest radius of curvature to the above list of parameters allows explaining 82% of the total variability of the mechanical response.

The remaining 18% are mainly explained by the interaction between muscle mechanical behaviour and (1) muscle thickness (4.5%), (2) external force (3.7%), and (3) fat thickness (1.3%). Thus, considering a fixed muscle mechanical behaviour, an increase of the maximum shear strain will result from an increase in the external force and/or a decrease in the muscle and fat thicknesses. This is consistent with the results reported by Oomens et al. (2003) and Portnoy et al. (2011).

Limitations and perspectives of this work are detailed herein. **First**, the fact that local shear strains predicted by the local FE model are all higher than those predicted by the reference FE model strains points at a systematic error. This may be partly due to the fact that approximating the ischial tuberosity by a torus is too gross and leads to biases in the mechanical response. Examination of the ischial tuberosities on the US images revealed that some subjects roughly had a triangular bore rather than a circular bore in shape. As discussed above, in indentation-like configurations, the geometry of the indenter is known to have a paramount importance. As far as the authors are aware of, analysis of the inter-individual variations of the morphological cross section of the ischial tuberosity has never been investigated before and further work is required to improve the geometric approximation of the ischial tuberosity from US images. The systematic error also suggests that, in addition to the choice of the geometric approximation of the ischial tuberosity, other factors involved in the definition and measurement of the principal shear strain in the local FE model might be lacking, their identification requiring further work. **Second**, the extraction of the material properties using an inverse identification method (for which the optimal parameters are obtained by minimizing the distance between experimental measures and numerical results), although popular for lower limb soft tissues (Affagard et al., 2015;



Frauziols et al., 2016; Macron et al., 2018; Rohan et al., 2014; Sadler et al., 2018), is not compatible with clinical implementation because of lengthy solver times for the models and the need for a trained user to develop and interpret the FE model. Ultrasound Elastography, and, in particular, Supersonic Shear Imaging (SSI) technique, is emerging as an innovative tool that could provide a quantitative evaluation of biomechanical properties of soft tissues (Eby et al., 2013; Genisson et al., 2010; Haen et al., 2017; Vergari et al., 2014). However, to our knowledge and to date, no correlation has been done between shear moduli obtained by Shear Wave Elastography and mechanical properties from classic *ex vivo* mechanical testing methods. The development of surrogate models that allow equivalent predictions to single FEA solutions, across a broad population with sufficiently reduced computational expense for clinical use (Steer et al., 2019) is a promising alternative that will be explored in future work. **Third**, the strain damage thresholds (above 75% and above 45%) reported in the literature for tissue injury (motivated by the work of Ceelen et al., 2008; Loerakker et al., 2011) come from animal models and should be *considered* with some caution since they might not be relevant for humans. Very recently, in an attempt to elucidate the soft tissue injuries leading from pressure-driven ischemia, a computational model linking microvascular collapse to tissue hypoxia in a multiscale model of Pressure Ulcer initiation has been proposed (Sree et al., 2019a, 2019b) in the context of Pressure Ulcer formation. These types of models, coupled with recent improvements in ultrasound imaging technologies that allow to measure tissue perfusion in clinical routine, constitute opportunities for elucidating some of the scientific challenges associated with the *customization* of the injury thresholds.

In the present contribution, the authors have used a multimodal approach based on B-mode ultrasound images and low-dose biplanar X-ray images in a non-weight-bearing sitting posture for the fast generation of patient-specific FE models of the buttock. Compared to previously conducted, MRI-based computational models (Al-Dirini et al., 2016; Levy et al., 2017; Levy and Gefen, 2017; Linder-Ganz et al., 2007, 2008, 2009; Moerman et al., 2017; Sopher et al., 2010; Zeevi et al., 2017), our protocol suffers from a number of limitations including the poor visibility of B-mode ultrasound for viewing the organization and composition of the buttock soft tissues (muscle groups, tendon, fat pads and ligament borders) and the limited field of view of B-mode ultrasound. However, most MRI-based computational models in the literature model these as a single homogenous material to allow for convergence of tissue geometry and, therefore, clearly fail to take advantage of the capacity of MRI to differentiate between the individual soft tissue structures. Moreover, long acquisition times of MR imaging prevent the representation of a realistic unloaded sitting position without resorting to devices such as: rubber tires (Linder-Ganz et al., 2007), inclined plane (Al-Dirini et al., 2016) and thigh and arms supports (Call et al., 2017). On the contrary, the proposed protocol allows reproducing the unloaded sitting position easily. Finally, acknowledging the fact that mechanical strains are responsible for deformation-induced damage involved in the initiation of Deep Tissue Injury (DTI), a better assessment of the internal behaviour could enable to enhance the modelling of the transmission of loads into the different structures composing the buttock. If MRI is a potential tool for the quantitative evaluation of subdermal soft tissue strains, it has important drawbacks including long acquisition time, examination cost and confined environment. On the contrary, in a recent publication (Doridam et al., 2018), we showed the feasibility of using B-mode ultrasound imaging for the quantification of internal soft-tissue strains of buttock tissues in two perpendicular planes during sitting. Further research is currently under progress to develop and validate computational modelling based on ultrasound data alone. This would make additional DTI research more accessible and attainable, and would allow for translational development of future patient-specific risk assessment tools.

This work proposed a promising new step towards estimating internal mechanical conditions within loaded soft tissues from data

potentially compatible with daily clinical routine. While additional experimental validation is required for the design of appropriate protocols for the robust extraction of both the morphological parameters of interest and the characterization of the mechanical behaviour of the soft tissue of interest, this work opens a way to overcome the barriers to clinical implementation of biomechanical metrics as surrogates for improving the management and prevention of PU including difficulty in obtaining imaging data.

#### Author contributions statement

AM, HP and PYR contributed to the conception and design of the study; JD, MJS and AM performed experiment and data collection; IR performed the statistics. All the authors contributed to data interpretation and preparation of the manuscript. All authors approved the final version of the manuscript.

#### Declaration of competing interest

The authors certify that no conflict of interest is raised by this work.

#### Acknowledgments

This work was supported by the Fondation de l'Avenir (grant number AP-RM-2016-030), by la Fondation des Arts et Métiers and the Fonds de dotation Clinatec. The authors are also grateful to the ParisTech BiomecAM chair program on subject-specific musculoskeletal modelling.

#### References

- Affagard, J.-S., Feissel, P., Bensamoun, S.F., 2015. Identification of hyperelastic properties of passive thigh muscle under compression with an inverse method from a displacement field measurement. *J. Biomech.* 48, 4081–4086. <https://doi.org/10.1016/j.jbiomech.2015.10.007>.
- Agam, L., Gefen, A., 2007. Pressure ulcers and deep tissue injury: a bioengineering perspective. *J. Wound Care* 16, 336–342. <https://doi.org/10.12968/jowc.2007.16.8.27854>.
- Akins, J.S., Vallye, J.J., Karg, P.E., Kopplin, K., Gefen, A., Poojary-Mazzotta, P., Brienza, D.M., 2016. Feasibility of freehand ultrasound to measure anatomical features associated with deep tissue injury risk. *Med. Eng. Phys.* 0, 1–6. <https://doi.org/10.1016/j.medengphy.2016.04.026>.
- Al-Dirini, R.M.A., Reed, M.P., Jingwen, H., Thewlis, D., 2016. Development and validation of a high anatomical fidelity FE model for the buttock and thigh of a seated individual. 44, 2805–2816. <https://doi.org/10.1007/s10439-016-1560-3>.
- Bercoff, J., Tanter, M., Fink, M., 2004. Supersonic shear imaging: a new technique for soft tissue elasticity mapping. *IEEE Trans. Ultrason. Ferroelectr. Freq. Control* 51, 396–409. <https://doi.org/10.1109/TUFFC.2004.1295425>.
- Bouten, C.V., Oomens, C.W., Baaijens, F.P., Bader, D.L., 2003. The etiology of pressure ulcers: skin deep or muscle bound? *Arch. Phys. Med. Rehabil.* 84, 616–619. <https://doi.org/10.1053/apmr.2003.50038>.
- Breuls, R.G.M., Bouten, C.V.C., Oomens, C.W.J., Bader, D.L., Baaijens, F.P.T., 2003. A theoretical analysis of damage evolution in skeletal muscle tissue with reference to pressure ulcer development. *J. Biomech. Eng.* 125, 902–909. <https://doi.org/10.1115/1.1634287>.
- Bucki, M., Luboz, V., Perrier, A., Champion, E., Diot, B., Vuillerme, N., Payan, Y., 2016. Clinical workflow for personalized foot pressure ulcer prevention. *Med. Eng. Phys.* 38, 845–853. <https://doi.org/10.1016/j.medengphy.2016.04.017>.
- Call, E., Hetzel, T., McLean, C., Burton, J.N., Oberg, C., 2017. Off loading wheelchair cushion provides best case reduction in tissue deformation as indicated by MRI. *J. Tissue Viability* 26, 172–179. <https://doi.org/10.1016/j.jtv.2017.05.002>.
- Ceelen, Stekelenburg, A., Mulders, J.L.J., Strijkers, G.J., Baaijens, F.P.T., Nicolay, K., Oomens, C.W.J., 2008. Validation of a numerical model of skeletal muscle compression with MR tagging: a contribution to pressure ulcer research. *J. Biomech. Eng.* 130, 061015–061018. <https://doi.org/10.1115/1.2987877>.
- Chow, W.W., Odell, E.L., 1978. Deformations and stresses in soft body tissues of a sitting person. *J. Biomech. Eng.* 100, 79–87. <https://doi.org/10.1115/1.3426196>.
- Dabnichki, P.A., Crocombe, A.D., Hughes, S.C., 1994. Deformation and stress analysis of supported buttock contact. *Proc. Inst. Mech. Eng. H* 208, 9–17. <https://doi.org/10.1177/095441199420800102>.
- Daniel, R.K., Priest, D.L., Wheatley, D.C., 1981. Etiologic factors in pressure sores: an experimental model. *Arch. Phys. Med. Rehabil.* 62, 492–498.
- Doridam, J., Macron, A., Vergari, C., Verney, A., Rohan, P.-Y., Pillet, H., 2018. Feasibility of sub-dermal soft tissue deformation assessment using B-mode ultrasound for pressure ulcer prevention. *J. Tissue Viability* 27, 238–243. <https://doi.org/10.1016/j.jtv.2018.08.002>.

- Eby, S.F., Song, P., Chen, S., Chen, Q., Greenleaf, J.F., An, K.-N., 2013. Validation of shear wave elastography in skeletal muscle. *J. Biomech.* 46, 2381–2387. <https://doi.org/10.1016/j.jbiomech.2013.07.033>.
- Frauziols, F., Chassagne, F., Badel, P., Navarro, L., Molimard, J., Curt, N., Avril, S., 2016. In vivo identification of the passive mechanical properties of deep soft tissues in the human leg. *Strain* 52, 400–411. <https://doi.org/10.1111/str.12204>.
- Gawlipta, D., Li, W., Oomens, C.W.J., Baaijens, F.P.T., Bader, D.L., Bouten, C.V.C., 2007. The relative contributions of compression and hypoxia to development of muscle tissue damage: an in vitro study. *Ann. Biomed. Eng.* 35, 273–284. <https://doi.org/10.1007/s10439-006-9222-5>.
- Gefen, A., 2011. How do microclimate factors affect the risk for superficial pressure ulcers: a mathematical modeling study. *J. Tissue Viability* 20, 81–88. <https://doi.org/10.1016/j.jtv.2010.10.002>.
- Gennisson, J.-L., Deffieux, T., Macé, E., Montaldo, G., Fink, M., Tanter, M., 2010. Viscoelastic and anisotropic mechanical properties of in vivo muscle tissue assessed by supersonic shear imaging. *Ultrasound Med. Biol.* 36, 789–801. <https://doi.org/10.1016/j.ultrasmedbio.2010.02.013>.
- Gennisson, J.-L., Deffieux, T., Fink, M., Tanter, M., 2013. Ultrasound elastography: principles and techniques. *Diagn. Interv. Imaging, Ultrasound elastography* 94, 487–495. <https://doi.org/10.1016/j.diii.2013.01.022>.
- Haen, T.X., Roux, A., Soubeyrand, M., Laporte, S., 2017. Shear waves elastography for assessment of human Achilles tendon's biomechanical properties: an experimental study. *J. Mech. Behav. Biomed. Mater.* 69, 178–184. <https://doi.org/10.1016/j.jmbbm.2017.01.007>.
- Kosiak, M., 1959. Etiology and pathology of ischemic ulcers. *Arch. Phys. Med. Rehabil.* 40, 62–69.
- Kosiak, M., 1961. Etiology of decubitus ulcers. *Arch. Phys. Med. Rehabil.* 42, 19–29.
- Levy, A., Gefen, A., 2017. Assessment of the biomechanical effects of prophylactic sacral dressings on tissue loads: a computational modeling analysis. *Ostomy Wound Manage* 63, 48–55.
- Levy, A., Schwartz, D., Gefen, A., 2017. The contribution of a directional preference of stiffness to the efficacy of prophylactic sacral dressings in protecting healthy and diabetic tissues from pressure injury: computational modelling studies. *Int. Wound J.* 14, 1370–1377. <https://doi.org/10.1111/iwj.12821>.
- Linder-Ganz, E., Shabshin, N., Itzhak, Y., Gefen, A., 2007. Assessment of mechanical conditions in sub-dermal tissues during sitting: a combined experimental-MRI and finite element approach. *J. Biomech.* 40, 1443–1454. <https://doi.org/10.1016/j.jbiomech.2006.06.020>.
- Linder-Ganz, E., Shabshin, N., Itzhak, Y., Yizhar, Z., Siev-Ner, I., Gefen, A., 2008. Strains and stresses in sub-dermal tissues of the buttocks are greater in paraplegics than in healthy during sitting. *J. Biomech.* 41, 567–580. <https://doi.org/10.1016/j.jbiomech.2007.10.011>.
- Linder-Ganz, E., Yarnitzky, G., Yizhar, Z., Siev-Ner, I., Gefen, A., 2009. Real-time finite element monitoring of sub-dermal tissue stresses in individuals with spinal cord injury: toward prevention of pressure ulcers. *Ann. Biomed. Eng.* 37, 387–400. <https://doi.org/10.1007/s10439-008-9607-8>.
- Loerakker, S., Stekelenburg, A., Strijkers, G.J., Rijpkema, J.J.M., Baaijens, F.P.T., Bader, D.L., Nicolay, K., Oomens, C.W.J., 2010. Temporal effects of mechanical loading on deformation-induced damage in skeletal muscle tissue. *Ann. Biomed. Eng.* 38, 2577–2587. <https://doi.org/10.1007/s10439-010-0002-x>.
- Loerakker, S., Manders, E., Strijkers, G.J., Nicolay, K., Baaijens, F.P.T., Bader, D.L., Oomens, C.W.J., 2011. The effects of deformation, ischemia, and reperfusion on the development of muscle damage during prolonged loading. *J. Appl. Physiol.* 111, 1168–1177. <https://doi.org/10.1152/jappphysiol.00389.2011>.
- Luboz, V., Petrizelli, M., Bucki, M., Diot, B., Vuillerme, N., Payan, Y., 2014. Biomechanical modeling to prevent ischial pressure ulcers. *J. Biomech.* 47, 2231–2236. <https://doi.org/10.1016/j.jbiomech.2014.05.004>.
- Luboz, V., Bailet, M., Boichon, C., Rochette, M., Diot, B., Bucki, M., Payan, Y., 2017. Personalized modeling for real-time pressure ulcer prevention in sitting posture. *J. Tissue Viability* 2–6. <https://doi.org/10.1016/j.jtv.2017.06.002>.
- Macron, A., Pillet, H., Doridam, J., Verney, A., Rohan, P.-Y., 2018. Development and evaluation of a new methodology for the fast generation of patient-specific Finite Element models of the buttock for sitting-acquired deep tissue injury prevention. *J. Biomech.* 79, 173–180. <https://doi.org/10.1016/j.jbiomech.2018.08.001>.
- Makhsous, M., Venkatasubramanian, G., Chawla, A., Pathak, Y., Priebe, M., Rymer, W.Z., Lin, F., 2008. Investigation of soft-tissue stiffness alteration in denervated human tissue using an ultrasound indentation system. *J. Spinal Cord Med.* 31, 88–96.
- Moerman, K.M., van Vijven, M., Solis, L.R., van Haften, E.E., Loenen, A.C.Y., Mushahwar, V.K., Oomens, C.W.J., 2017. On the importance of 3D, geometrically accurate, and subject-specific finite element analysis for evaluation of in-vivo soft tissue loads. *Comput. Methods Biomech. Biomed. Engin.* 20, 483–491. <https://doi.org/10.1080/10255842.2016.1250259>.
- Nelissen, J.L., Traa, W.A., de Boer, H.H., de Graaf, L., Mazzoli, V., Savci-Heijink, C.D., Nicolay, K., Froeling, M., Bader, D.L., Nederveen, A.J., Oomens, C.W.J., Strijkers, G.J., 2018. An advanced magnetic resonance imaging perspective on the etiology of deep tissue injury. *J. Appl. Physiol.* 124, 1580–1596. <https://doi.org/10.1152/jappphysiol.00891.2017>.
- NPUAP/EPUAP, 2009. *Prevention and Treatment of Pressure Ulcers: Clinical Practice Guidelines*.
- Oomens, C.W.J., Bressers, O.F.J.T., Bosboom, E.M.H., Bouten, C.V.C., Blader, D.L., 2003. Can loaded interface characteristics influence strain distributions in muscle adjacent to bony prominences? *Comput. Methods Biomech. Biomed. Engin.* 6, 171–180. <https://doi.org/10.1080/1025584031000121034>.
- Oomens, C.W.J., Bader, D.L., Loerakker, S., Baaijens, F., 2015. Pressure induced deep tissue injury explained. *Ann. Biomed. Eng.* 43, 297–305. <https://doi.org/10.1007/s10439-014-1202-6>.
- Oomens, C.W.J., Broek, M., Hemmes, B., Bader, D.L., 2016. How does lateral tilting affect the internal strains in the sacral region of bed ridden patients? — a contribution to pressure ulcer prevention. *Clin. Biomech.* 35, 7–13. <https://doi.org/10.1016/j.clinbiomech.2016.03.009>.
- Portnoy, S., Vuillerme, N., Payan, Y., Gefen, A., 2011. Clinically oriented real-time monitoring of the individual's risk for deep tissue injury. *Med. Biol. Eng. Comput.* 49, 473–483. <https://doi.org/10.1007/s11517-011-0754-y>.
- Reswick, J.B., Rogers, J.E., 1976. Experience at rancho los amigos hospital with devices and techniques to prevent pressure sores. In: *Bed Sore Biomechanics, Strathclyde Bioengineering Seminars*. Palgrave, London, pp. 301–310. [https://doi.org/10.1007/978-1-349-02492-6\\_38](https://doi.org/10.1007/978-1-349-02492-6_38).
- Rohan, P.-Y., Badel, P., Lun, B., Rastel, D., Avril, S., 2014. Prediction of the biomechanical effects of compression therapy on deep veins using finite element modelling. *Ann. Biomed. Eng.* 43, 314–324. <https://doi.org/10.1007/s10439-014-1121-6>.
- Sadler, Z., Scott, J., Drost, J., Chen, S., Roccabianca, S., Bush, T.R., 2018. Initial estimation of the in vivo material properties of the seated human buttocks and thighs. *Int. J. Non-Linear Mech.* 107, 77–85. <https://doi.org/10.1016/j.ijnonlinmec.2018.09.007>.
- Simo, J.C., Taylor, R.L., 1991. Quasi-incompressible finite elasticity in principal stretches. Continuum basis and numerical algorithms\* (Juan C. SIMO).
- Sopher, R., Nixon, J., Gorecki, C., Gefen, A., 2010. Exposure to internal muscle tissue loads under the ischial tuberosities during sitting is elevated at abnormally high or low body mass indices. *J. Biomech.* 43, 280–286. <https://doi.org/10.1016/j.jbiomech.2009.08.021>.
- Sopher, R., Nixon, J., Gorecki, C., Gefen, A., 2011. Effects of intramuscular fat infiltration, scarring, and spasticity on the risk for sitting-acquired deep tissue injury in spinal cord injury patients. *J. Biomech. Eng.* 133. <https://doi.org/10.1115/1.4003325>.
- Sree, V.D., Rausch, M.K., Tepole, A.B., 2019a. Towards understanding pressure ulcer formation: coupling an inflammation regulatory network to a tissue scale finite element model. *Mech. Res. Commun.* 97, 80–88. <https://doi.org/10.1016/j.mechrescom.2019.05.003>.
- Sree, V.D., Rausch, M.K., Tepole, A.B., 2019b. Linking microvascular collapse to tissue hypoxia in a multiscale model of pressure ulcer initiation. *Biomech. Model. Mechanobiol.* <https://doi.org/10.1007/s10237-019-01187-5>.
- Steer, J.W., Worsley, P.R., Browne, M., Dickinson, A.S., 2019. Predictive prosthetic socket design: part 1—population-based evaluation of transtibial prosthetic sockets by FEA-driven surrogate modelling. *Biomech. Model. Mechanobiol.* <https://doi.org/10.1007/s10237-019-01195-5>.
- Stekelenburg, A., Oomens, C.W.J., Strijkers, G.J., de Graaf, L., Bader, D.L., Nicolay, K., 2006. A new MR-compatible loading device to study in vivo muscle damage development in rats due to compressive loading. *Med. Eng. Phys.* 28, 331–338. <https://doi.org/10.1016/j.medengphy.2005.07.005>.
- Stekelenburg, A., Strijkers, G.J., Parusel, H., Bader, D.L., Nicolay, K., Oomens, C.W., 2007. Role of ischemia and deformation in the onset of compression-induced deep tissue injury: MRI-based studies in a rat model. *J. Appl. Physiol.* 102, 2002–2011. <https://doi.org/10.1152/jappphysiol.01115.2006>.
- Swaine, J.M., Moe, A., Bredahl, W., Bader, D.L., Oomens, C.W.J., Lester, L., O'Loughlin, E., Santamaria, N., Stacey, M.C., 2017. Adaptation of a MR imaging protocol into a real-time clinical biometric ultrasound protocol for persons with spinal cord injury at risk for deep tissue injury: a reliability study. *J. Tissue Viability* 27, 32–41. <https://doi.org/10.1016/j.jtv.2017.07.004>.
- Vergari, C., Rouch, P., Dubois, G., Bonneau, D., Dubouset, J., Tanter, M., Gennisson, J.-L., Skalli, W., 2014. Intervertebral disc characterization by shear wave elastography: an in vitro preliminary study. *Proc. Inst. Mech. Eng. H* 228, 607–615. <https://doi.org/10.1177/0954411914540279>.
- Zeevi, T., Levy, A., Brauner, N., Gefen, A., 2017. Effects of ambient conditions on the risk of pressure injuries in bedridden patients-multi-physics modelling of microclimate. *Int. Wound J.* <https://doi.org/10.1111/iwj.12877>.